Article

Thermal Effect on the Instability of Annular Liquid Jet

Xiao Cui and Boqi Jia *

School of Astronautics, Beihang University, Beijing 102206, China; cuixiao@buaa.edu.cn
* Correspondence: jiabq@buaa.edu.cn

Abstract: The linear instability of an annular liquid jet with a radial temperature gradient in an inviscid gas steam is investigated theoretically. A physical model of an annular liquid jet with a radial temperature gradient is established, dimensionless governing equations and boundary conditions are given, and numerical solutions are obtained using the spectral collocation method. The correctness of the results is verified to a certain extent. The liquid surface tension coefficient is assumed to be a linear function of temperature. The effects of various dimensionless parameters (including the Marangoni number/Prandtl number, Reynolds number, temperature gradient, Weber number, gas-to-liquid density ratio and velocity ratio) on the instability of the annular liquid jet are discussed. A decreasing Weber number destabilizes the annular liquid jet when the Weber number is lower than a critical value. It is found that the effects of the Marangoni effect are related to the Weber number. The Marangoni effect enhances instability when the Weber number is small, while the Marangoni effect weakens instability when the Weber number is large. In addition, because the thermal effect is considered, a decreasing Reynolds number enhances the instability when the Weber number is lower than a critical value, which is similar to the results of a viscous liquid sheet with a temperature difference between two planar surfaces. Furthermore, the effects of other dimensionless parameters are also investigated.

Keywords: thermal effect; linear instability analysis; annular liquid jet

1. Introduction

The breakup of a liquid jet is encountered in various applications, such as liquid rocket engines and gas turbines [1]. The instability of a liquid jet, resulting in breakup, is a classical fluid dynamic problem dating back to Rayleigh [2], who first developed the linear stability analysis method to investigate the instability of liquid jets, neglecting the liquid viscosity and aerodynamic effects. Crapper et al. [3] studied the instability of an inviscid annular jet injecting into a stationary gas medium. They obtained the dispersion equation and numerically solved it. In their research, they mentioned that there are two solutions for the perturbation growth rate. Shen and Li [4] studied the sinusoidal mode and the varicose mode of the flat liquid film and proposed the "para-sinuous mode" and "para-varicose mode"; they found that the outer and inner amplitude ratio is not an invariant, which was opposite to the assumption made by Meyer and Weihs [5]. Chen and Lin [6] investigated the instability of an annular jet surrounded by a viscous gas in a pipe. Considering practical spray applications [7,8], aerodynamic and swirling effects were also studied [9–13]. Due to a smaller Mach number, the compressibility of gas is usually neglected. However, the compressibility of gas plays a significant role in the instability of the gas–liquid interface [14,15]; a higher gas Mach number is a destabilizing parameter and enhances the breakup process of an annular liquid jet [16,17]. As there is a temperature gradient in practical applications, the thermal effect, which is neglected in the above studies, is also considered in theoretical research [18]. The effects of the Biot number and the deviation of surface tension caused by the temperature gradient were investigated by Funada [19]. Oron et al. [20] investigated the instability of the sinuous mode when the Marangoni and Crispation numbers are different at the cold and hot surfaces in the

case of a zero Biot number. Davalos-Orozco [21] studied the thermocapillary instability of a Newtonian liquid sheet moving in a motionless gas ambient. They found that the liquid sheet becomes more unstable when a temperature difference exists, and liquid viscosity destabilizes the sheet under this condition. Following their study, Tong et al. [22] investigated the thermocapillary instability behavior of planar liquid sheets when the elastic effect was introduced. The spatial–temporal instability behavior of a viscous liquid sheet with a temperature difference between the two surfaces was investigated theoretically [23]. The effect of centrifugal force on the thermocapillary instability of a liquid sheet was examined by Zhang et al. [24]. The problem of capillary jet breakup was investigated in the context of temporal instability [25]. The effects of axial and radial temperature gradients were also considered [26–28].

In the present study, we aim to theoretically investigate the instability of an annular liquid jet in an inviscid gas stream. A physical model of an annular liquid jet with a radial temperature gradient is established; the temporal linear instability theory is employed to examine the thermal effects on annular liquid jet instability. The process parameters are therefore chosen in a wide range of values. The paper is organized as follows: In Section 2, the theoretical model of an annular liquid jet with a radial temperature gradient is described; dimensionless governing equations and boundary conditions are also expressed. In Section 3, numerical solutions are obtained using the spectral collocation method, and variations in the growth rate with a wavenumber for the annular liquid jet in unstable modes are presented. In addition, the effects of the direction of the temperature gradient, as well as the main parameters, on the jet instability are also discussed. In Section 4, the main conclusions are drawn.

2. Theoretical Model

As depicted in Figure 1, this paper considers a two-dimensional annular liquid jet injected into a gas medium, and both liquid and gas are incompressible. The densities of the inner and outer gas and liquid phases are ρ_1, ρ_2, and ρ_l, respectively; gas velocities in axial and radial directions are $(U_1, 0)$ and $(U_2, 0)$, $(U_l, 0)$. The temperatures of the inner and outer gas are T_1 and T_2, and the basic pressures of the liquid and gas phases are constant. The liquid viscosity is μ, and the thermal diffusivity of liquid is κ. Assuming that the heat fluxes at $r = R_1$ and $r = R_2$ are constant, the temperatures at the inner and outer gas–liquid interfaces are T_1 and T_2 and the surface tensions are σ_1 and σ_2, respectively.
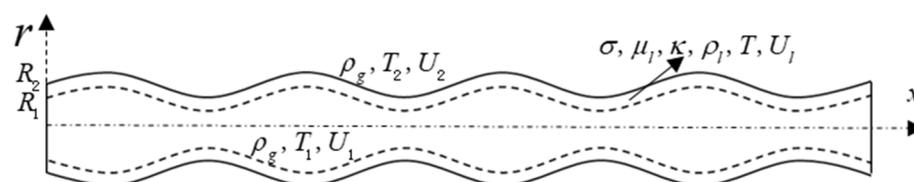

Figure 1. Schematic of the profile of the annular liquid jet.

In the present study, the method of linear stability analysis is used to investigate the initiation of the instability process; the flow field is disturbed with the disturbance quantities $\mathbf{u}$, p and $\widetilde{T}$ on the basic quantities $\mathbf{U}$, $\overline{P}$ and $\overline{T}$. Therefore, the perturbed flow fields are as follows:

$$\left(\mathbf{U}_j, P_j, \mathbf{U}_l, P_l, T\right) = \left(\overline{\mathbf{U}}_j, \overline{P}_j, \overline{\mathbf{U}}_l, \overline{P}_l, \overline{T}\right) + \left(\mathbf{u}_j, p_j, \mathbf{u}_l, p_l, \widetilde{T}\right) \tag{1}$$

where $j = 1, 2$ indicates the inner and outer gas phases, and $\overline{\mathbf{U}}_j$ and $\overline{\mathbf{U}}_l$ are the velocity vectors of the gas and liquid phases, respectively.

Due to the temperature difference between the inner and outer gas–liquid interface, there is a temperature gradient in the liquid phase. For steady-state conditions with no heat generation, the expression of the temperature gradient in the liquid phase is as follows [29]:

$$\lambda = \frac{\partial \overline{T}}{\partial r} = \frac{\Delta \overline{T}}{r \ln(R_2 / R_1)} \tag{2}$$

In the present study, the surface tension is a physical parameter dependent on temperature, which is similar to previous studies; the expression is as below:

$$\sigma_2 = \sigma_1 - \beta(T_2 - T_1) = \beta T_0 - \beta(T_2 - T_1) = \beta(T_0 - \Delta T) \tag{3}$$

where β is a constant presenting the rate of the surface tension coefficient with temperature variation; in fact, T_0 is decided by σ_1 and β. Here, we replace σ_1 with βT_0 for a convenient calculation and to obtain the form $\sigma_2 = \beta(T_0 - \Delta T)$.

To make the results more universal, the appropriate velocity and length scales for both gas and liquid are used to transform variables into dimensionless form, yielding the following:

$$\begin{aligned}
&Re = \frac{\rho_l \overline{U}_l (R_2 - R_1)}{\mu}, We_1 = \frac{\rho_l \overline{U}_l^2 (R_2 - R_1)}{\sigma_1}, We_2 = \frac{\rho_l \overline{U}_l^2 (R_2 - R_1)}{\sigma_2}, \\
&Pr = \frac{\mu}{\rho_l \kappa}, Ma = \frac{T_0 \beta (R_2 - R_1)}{\mu \kappa} \\
&\gamma_1 = \frac{\overline{U}_1}{\overline{U}_l}, \gamma_2 = \frac{\overline{U}_2}{\overline{U}_l}, \varepsilon_1 = \frac{\rho_1}{\rho_l}, \varepsilon_2 = \frac{\rho_2}{\rho_l}, \eta_1^* = \frac{\eta_1}{R_1}, \eta_2^* = \frac{\eta_2}{R_1}, u_l^* = \frac{u_l}{\overline{U}_l} \\
&v_l^* = \frac{v_l}{\overline{U}_l}, \varphi_1^* = \frac{\phi_1}{\overline{U}_l R_1}, \varphi_2^* = \frac{\varphi_2}{\overline{U}_l R_1}, p_l^* = \frac{p_l}{\rho_l \overline{U}_l^2}, p_1^* = \frac{p_1}{\rho_l \overline{U}_l^2}, p_2^* = \frac{p_2}{\rho_l \overline{U}_l^2} \\
&\widetilde{T}^* = \frac{\widetilde{T}}{\overline{T}_0}, t^* = \frac{\overline{U}_l t}{R_1}, x^* = \frac{x}{R_1}, r^* = \frac{r}{R_1}, \alpha = \frac{R_2}{R_1}, \Delta T^* = \frac{\Delta \overline{T}}{\overline{T}_0}, \lambda^* = \frac{\Delta T^*}{r^* \ln \alpha}
\end{aligned} \tag{4}$$

where Re is the Reynolds number of liquid, We_j is the Weber numbers of inner and outer gas–liquid interfaces, Pr is the Prandtl number, Ma is the Marangoni number, γ_1 is the velocity ratio of inner gas to liquid, γ_2 is the velocity ratio of outer gas to liquid, ε_1 is the density ratio of inner gas to liquid, ε_2 is the density ratio of outer gas to liquid, λ^* is the temperature gradient in the annular liquid jet, and ΔT^* is the dimensionless temperature difference between outer and inner gas–liquid interfaces. η_1^* and η_2^* are the dimensionless initiation of a disturbance at the inner and outer gas–liquid interfaces, respectively.

The physical quantities consist of basic and disturbance quantities in the linear stability analysis. Disturbance quantities are also infinitely small, ignoring the second- or higher order terms when governing equations are linearized. The governing equations are presented below.

Inner gas phase $(0 < r^* < 1)$,

The inner gas is inviscid and incompressible; the potential flow is subject to the continuity equation [30–32]:

$$\nabla \mathbf{u}_1^* = \nabla^2 \varphi_1^* = 0 \tag{5}$$

The potential flow of incompressible and inviscid fluids satisfies the NS equations and can be reduced to Bernoulli's equation. Therefore, the dimensionless pressure disturbance of the inner gas phase can be written as follows:

$$p_1^* = -\varepsilon_1 \left(\frac{\partial \varphi_1^*}{\partial t^*} + \gamma_1 \frac{\partial \varphi_1^*}{\partial x^*} \right) \tag{6}$$

The viscosity of the liquid is considered, and the governing equations of continuity and momentum conservation are as follows:

$$\frac{v_l^*}{r^*} + \frac{\partial v_l^*}{\partial r^*} + \frac{\partial u_l^*}{\partial x^*} = 0 \tag{7}$$

$$\frac{\partial u_l^*}{\partial t^*} + \frac{\partial u_l^*}{\partial x^*} = -\frac{\partial p_l^*}{\partial x^*} + \frac{1}{Re}\nabla^2 u_l^* \tag{8}$$

$$\frac{\partial v_l^*}{\partial t^*} + \frac{\partial v_l^*}{\partial x^*} = -\frac{\partial p_l^*}{\partial x^*} + \frac{1}{Re}\left(\nabla^2 v_l^* - \frac{v_l^*}{r^{*2}}\right) \tag{9}$$

Since there is a temperature gradient in an annular liquid jet, the energy balance equation should be considered:

$$\frac{\partial \widetilde{T}^*}{\partial t^*} + \frac{\partial \widetilde{T}^*}{\partial x^*} + v_l^* \lambda^* = \frac{1}{Re \cdot Pr}\nabla^2 \widetilde{T}^* \tag{10}$$

For the inner inviscid and incompressible gas, the governing equations are similar to those of the inner gas as below:

$$\nabla \mathbf{u}_2 = \nabla^2 \varphi_2^* = 0 \tag{11}$$

$$p_2^* = -\varepsilon_2\left(\frac{\partial \varphi_2^*}{\partial t^*} + \gamma_2 \frac{\partial \varphi_2^*}{\partial x^*}\right) \tag{12}$$

Boundary condition at $r^* \to 0$:

$$\frac{\partial \varphi_1^*}{\partial r^*} = \text{finite at } r^* \to 0 \tag{13}$$

$$p_2^* = -\varepsilon_2\left(\frac{\partial \varphi_2^*}{\partial t^*} + \gamma_2 \frac{\partial \varphi_2^*}{\partial x^*}\right) \tag{14}$$

Boundary conditions at $r^* = 1$:

$$v_l^* = \frac{\partial \eta_1^*}{\partial t^*} + \frac{\partial \eta_1^*}{\partial x^*} \text{ at } r^* = 1 \tag{15}$$

$$\frac{\partial u_l^*}{\partial r^*} + \frac{\partial v_l^*}{\partial x^*} = -\frac{Ma}{Re \cdot Pr}\frac{\partial \widetilde{T}^*}{\partial x^*} \text{ at } r^* = 1 \tag{16}$$

$$\frac{\partial \widetilde{T}^*}{\partial r^*} = 0 \text{ at } r^* = 1 \tag{17}$$

$$-p_l^* + \frac{2}{Re}\frac{\partial v_l^*}{\partial r^*} = -\frac{1}{We_1}\left(\eta_1^* + \frac{\partial^2 \eta_1^*}{\partial x^{*2}}\right) - p_1^* \text{ at } r^* = 1 \tag{18}$$

Boundary conditions at $r^* = \alpha$:

$$\frac{\partial \varphi_2^*}{\partial r^*} = \frac{\partial \eta_2^*}{\partial t^*} + \gamma_2 \frac{\partial \eta_2^*}{\partial x^*} \text{ at } r^* = \alpha \tag{19}$$

$$v_2^* = \frac{\partial \eta_2^*}{\partial t^*} + \frac{\partial \eta_2^*}{\partial x^*} \text{ at } r^* = \alpha \tag{20}$$

$$\frac{\partial u_l^*}{\partial r^*} + \frac{\partial v_l^*}{\partial x^*} = -\frac{Ma}{Re \cdot Pr}\frac{\partial \widetilde{T}^*}{\partial x^*} \text{ at } r^* = \alpha \tag{21}$$

$$\frac{\partial \widetilde{T}^*}{\partial r^*} = 0 \text{ at } r^* = \alpha \tag{22}$$

$$-p_l^* + \frac{2}{Re}\frac{\partial v_l^*}{\partial r^*} = \frac{1}{We_2}\left(\frac{\eta_2^*}{\alpha^2} + \frac{\partial^2 \eta_2^*}{\partial x^{*2}}\right) - p_2^* \text{ at } r^* = \alpha \tag{23}$$

Boundary condition at $r^* \to \infty$:

$$\frac{\partial \varphi_2^*}{\partial r} = 0 \text{ at } r^* \to \infty \tag{24}$$

Equations (16) and (21) and shear stress balance conditions predict that viscous shear stress is balanced by the surface tension gradient at the gas–liquid interface. Furthermore, the normal stress balance equations at the inner and outer gas–liquid interfaces are expressed by Equations (18) and (23).

The relational expression of the Weber number at the inner and outer interfaces when heat transfers from the outer to the inner gas phase is as follows:

$$We_2 = We_1 / (1 - \Delta T^*) \tag{25}$$

If the heat transfers from the inner to the outer gas phase, the relational expression is as below:

$$We_1 = We_2 / (1 + \Delta T^*) \tag{26}$$

3. Results and Discussion

3.1. Results of the Basic Case

The expressions of disturbance quantities in the linear stability analysis are harmonic and can be expressed as follows:

$$\left(\varphi_j^*, p_j^*, \mathbf{u}_l^*, p_l^*, \widetilde{T}^*, \eta_1^*, \eta_2^* \right) = \left(\hat{\varphi}_j^*, \hat{p}_j^*, \hat{\mathbf{u}}_l^*, \hat{p}_l^*, \hat{T}^*, \hat{\eta}_1^*, \hat{\eta}_2^* \right) \exp(\Omega t^* + iKx^*) \tag{27}$$

where $i = \sqrt{-1}$ is the imaginary unit. $\Omega = \Omega_r + \Omega_i$ is the dimensionless complex growth rate, where the real part Ω_r represents the growth rate of disturbance, and the imaginary part Ω_i is related to the disturbance frequency. K is the dimensionless wave number, which is related to the disturbance wavelength l by the relative expression $l = 2\pi / K$.

In the present study, the spectral collocation method, adopted in many papers [33–37], is used to obtain numerical solutions, and the details are not given. To verify the correctness of the model and program, the annular liquid jet without the thermal effect case is recalculated in our program by the settings $Ma = 0$, $\Delta T^* = 0$ and $We_1 = We_2 = We$, which was also calculated based on the analytical dispersion relation in Shen and Li [4]. The corresponding comparison is displayed in Figure 2. Clearly, the two resultant curves completely coincide with each other. This validates the present program.

In Figure 2, the curves display a relationship between the dimensionless wave number and the growth rate. The growth rate curves are normal, as the curves increase monotonously until the maximum growth rate is reached; after the maximum value is reached, the curves decrease and reach the axis of abscissa. The instability range is the wave number from zero to the abscissa crossing point, and the wave number corresponding to the abscissa crossing point is called the cutoff wave number. In addition, the research on the complex amplitudes shows two unstable modes, which are called "para-sinuous" (Figure 3a) and "para-varicose" (Figure 3b) [4]. The results show that the "para-sinuous" mode is more unstable than the "para-varicose" mode; i.e., the annular liquid jet breaks up more easily in the "para-sinuous" mode than in the "para-varicose" mode. Therefore, only the "para-sinuous" mode is discussed.

3.2. Effect of the Weber Number

Figure 4 shows the effect of the Weber number on the annular liquid jet instability. When heat transfers from the outer to the inner gas phase, the relational expression of the Weber number at the inner and outer interfaces increases from 40 to 4000, and the other parameters are constant. As shown in Figure 4, the maximum growth rate decreases with an increased Weber number when the wave number is small. However, as the wave number is larger than a critical value, the maximum unstable growth rate increases with an increase in the Weber number. Several pieces of research have reported this phenomenon. Similar to the breakup process of the liquid jet [38], surface tension is a main factor in the case of low Weber numbers, while it suppresses instability at large Weber numbers. When the Weber number is lower than the critical value, a decreasing Weber number destabilizes

the capillary instability, which plays a dominant role in this case. When the Weber number is larger than the critical value, the aerodynamic effect plays the central role in making the gas–liquid interface more unstable; therefore, increasing the Weber number enhances the annular liquid jet instability [4].
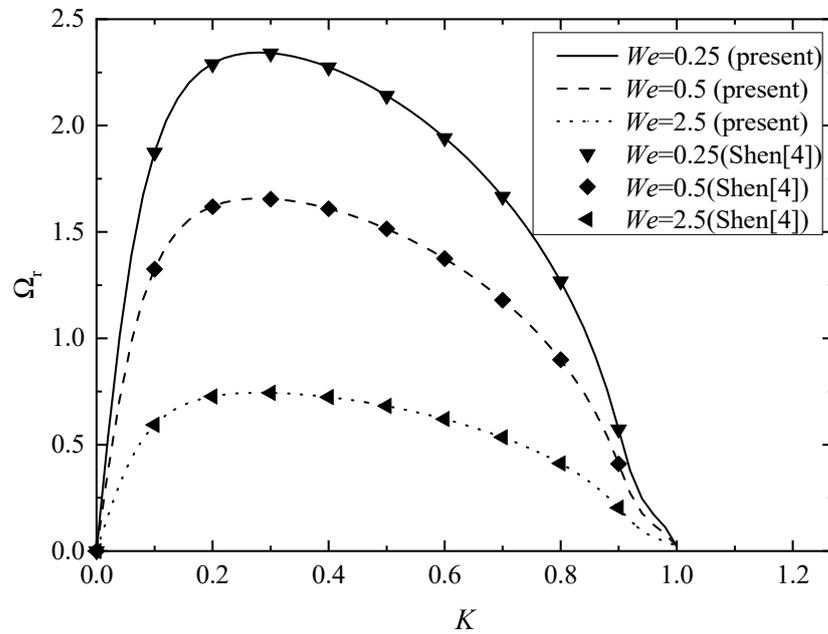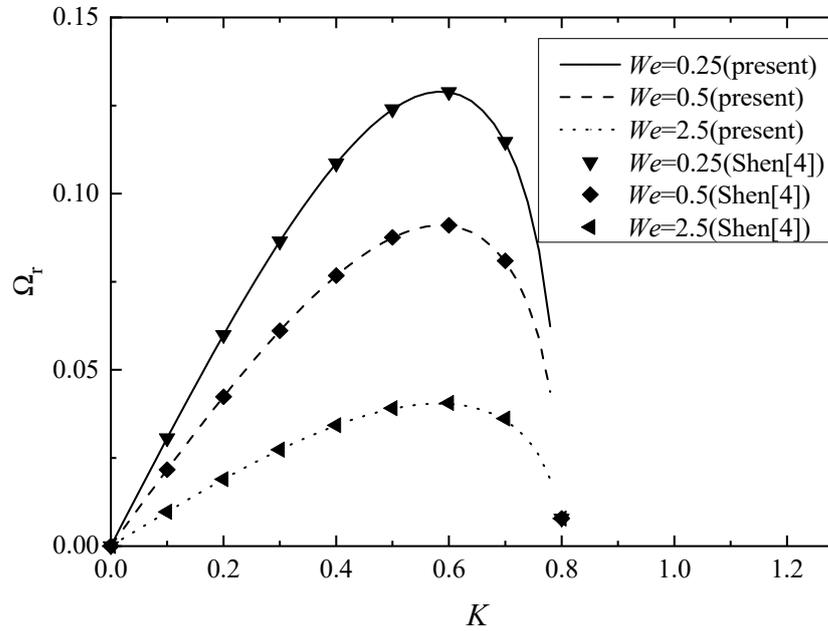
Figure 2. The results compared with Shen and Li in different modes: (**a**) "para-sinuous" mode and (**b**) "para-varicose" mode ($\alpha = 1.25$, $Re = 250$, $\varepsilon_1 = \varepsilon_2 = 0.001$).
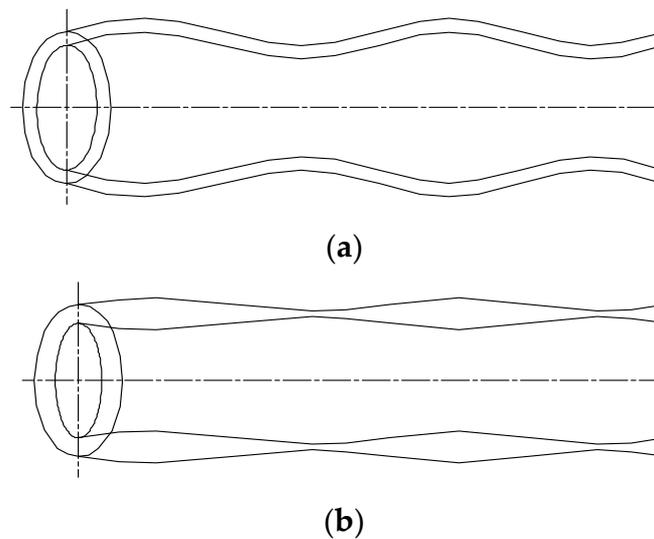
Figure 3. Different modes of annular liquid jet: (**a**) "para-sinuous" mode and (**b**) "para-varicose" mode.
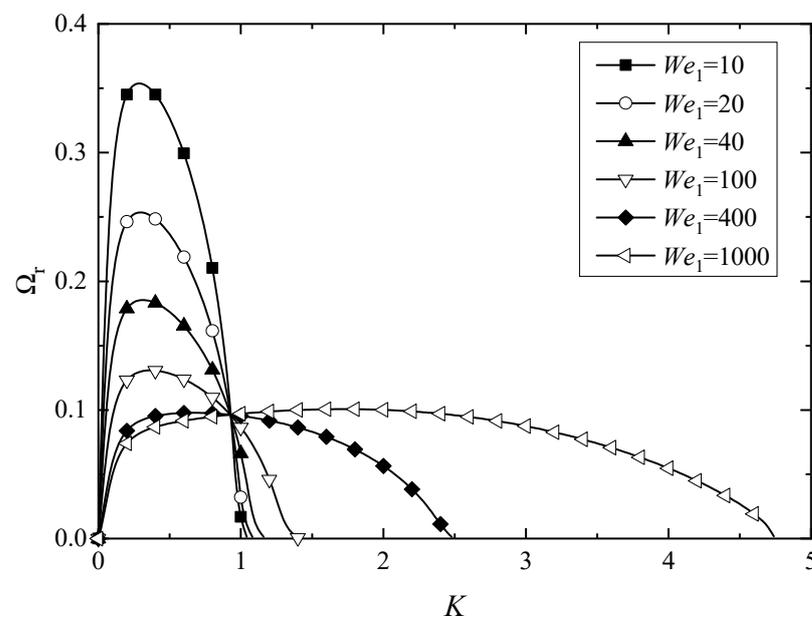
Figure 4. Effect of Weber number on the annular liquid jet instability ($Re = 25$, $We_2 = We_1/(1 - \Delta T^*)$, $\gamma_1 = \gamma_2 = 0$, $\varepsilon_1 = \varepsilon_2 = 0.001$, $Pr = 0.5$, $\Delta T^* = 0.2$, $\alpha = 1.25$, $Ma = 0.25$).

3.3. Marangoni Effects on Annular Liquid Jet Instability

When there is a radial temperature gradient in an annular liquid jet, the Marangoni effect will arise simultaneously. In the present study, the Marangoni number is defined as $Ma = T_0 \beta R_1 / \mu \kappa$, weighing the relative importance of thermal surface tension to viscosity and heat diffusion effects. It should be noted that the thermal effect affects the annular liquid jet instability through the shear stress balance conditions (Equations (15) and (20)), surface tension (Equations (25) and (26)) and normal stress balance conditions (Equations (17) and (22)).

The physical mechanism can be seen clearly in Figure 5, by which the thermal effect impacts the annular liquid jet instability; four different cases are calculated by modifying the program when the Weber number is small:

Case i: $We_1 = We_2 = 10$ and $Ma = 0$;
Case ii: $We_1 = We_2 = 10$ and $Ma = 0.25$;
Case iii: $We_1 = 10$, $We_2 = 12.5$ and $Ma = 0$;
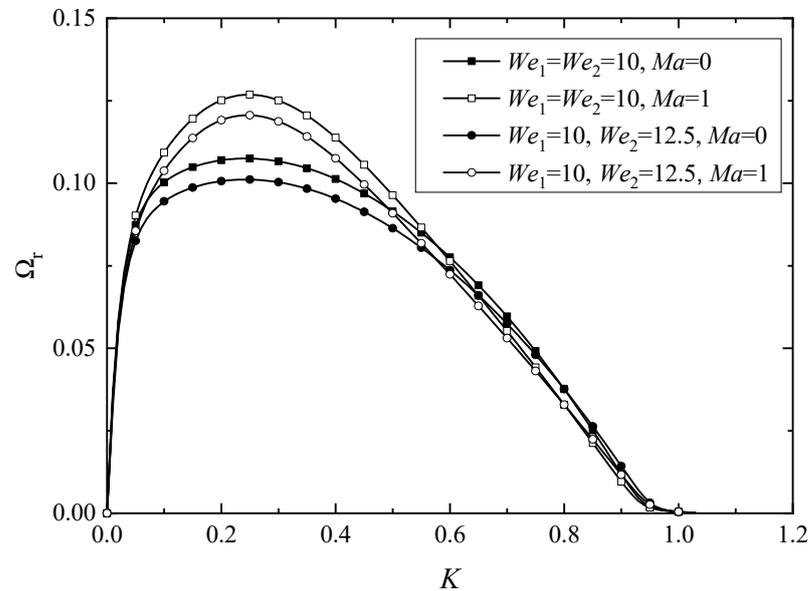Case iv: $We_1 = 10$, $We_2 = 50$ and $Ma = 0.25$.

Figure 5. Thermal effects when Weber number is small ($Re = 5$, $\gamma_1 = \gamma_2 = 0$, $\varepsilon_1 = \varepsilon_2 = 0.001$, $Pr = 0.5$, $\Delta T^* = 0.2$, $\alpha = 1.25$).

As shown in Figure 5, the unstable growth rate decreases in case iii compared with case i. Compared with case i, the maximum growth rate increases in case ii; the Marangoni effect enhances the instability of the annular liquid jet. The maximum growth rate in case iv is larger than that in case iii, while it is lower than that in case ii. Surface tension is a main factor in the case of low Weber numbers, and increasing the Weber number weakens capillary instability. Therefore, increasing We_2 decreases the disturbance growth when the Weber number is small, which can be seen in cases i and iii. As the Marangoni effect makes the liquid flow from the direction of low surface tension to high tension [18,28], capillary instability is enhanced. Thus, the annular liquid jet tends to be more unstable, which can be seen from cases iii and iv in Figure 5.

Similar to the cases of the small Weber number, four different cases are calculated when the Weber number is large:

Case v: $We_1 = We_2 = 1000$ and $Ma = 0$;
Case vi: $We_1 = We_2 = 1000$ and $Ma = 0.25$;
Case vii: $We_1 = 1000$, $We_2 = 1250$ and $Ma = 0$;
Case viii: $We_1 = 1000$, $We_2 = 1250$ and $Ma = 0.25$;

It can be clearly seen in Figure 6 that, comparing cases vii and viii, the maximum growth rate decreases. The Marangoni effect decreases the instability of the annular liquid jet. The maximum growth increases in cases v and vii; the same result can be obtained by comparing vi and viii. Here, it is important to know that the Weber number represents the aerodynamic force and the Marangoni number shows the thermal effect. When the Weber number is large, it is easy to observe that the aerodynamic force plays a dominant role in making the gas–liquid interface become more unstable, and increasing surface tension has a stabilizing effect on the gas–liquid interface. Hence, increasing We_2 enhances the instability of the annular liquid jet, and the Marangoni effect has a stabilizing effect on the gas–liquid interface.
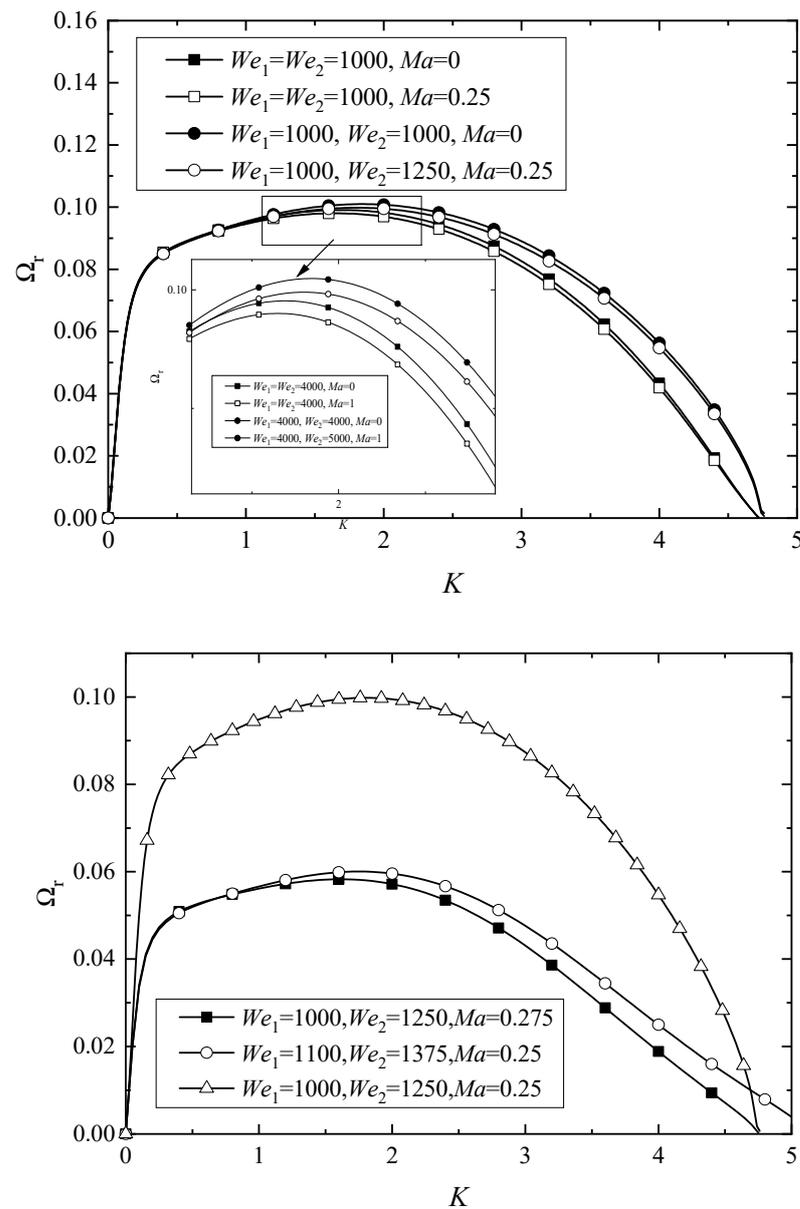
Figure 6. Marangoni effect when Weber number is large ($Re = 5$, $\gamma_1 = \gamma_2 = 0$, $\varepsilon_1 = \varepsilon_2 = 0.001$, $Pr = 0.5$, $\Delta T^* = 0.2$, $\alpha = 1.25$).

3.4. Effect of Prandtl Number

As shown in Figure 7, the maximum growth rate decreases with an increased Prandtl number at $Ma = 0.25$, while the instability range remains unchanged. The results suggest that the Prandtl number is a stabilizing factor, causing the annular liquid jet to be more stable when $Re = 0.5$. Meanwhile, similar to the results of Tong et al. [22], increasing the Prandtl number has no impact on the unstable growth rate in the case $Ma = 0$. However, when $Re = 5$, as shown in Figure 8, increasing the Prandtl number enhances the instability. It can be concluded that the influence of the Prandtl number on the annular liquid jet instability depends on the Marangoni number. Moreover, comparing Figures 7 and 8, the effect of viscidity is relative to the Reynolds number, which can be seen in Figure 9.
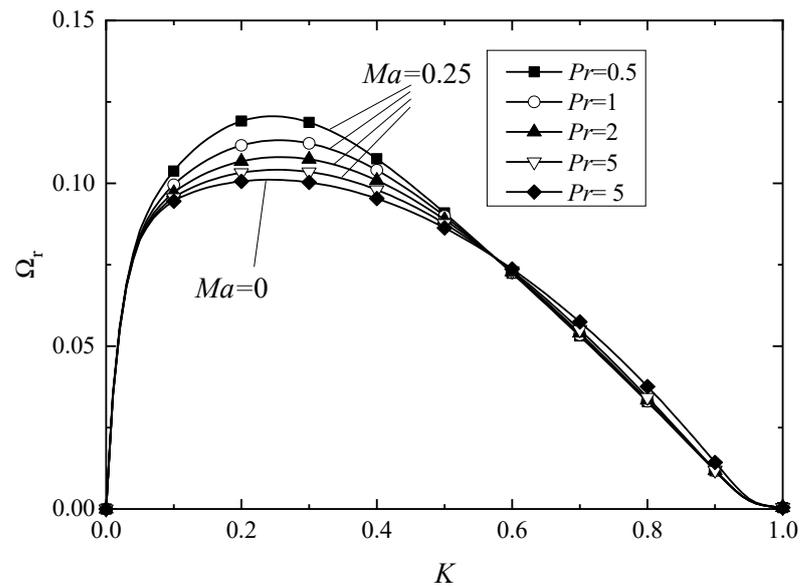
Figure 7. Effect of Prandtl number on the annular liquid jet instability when $Re = 0.5$ ($Re = 0.5$, $We_1 = 10$, $We_2 = 12.5$, $\gamma_1 = \gamma_2 = 0$, $\varepsilon_1 = \varepsilon_2 = 0.001$, $\Delta T^* = 0.2$, $\alpha = 1.25$, $Ma = 0.25$).
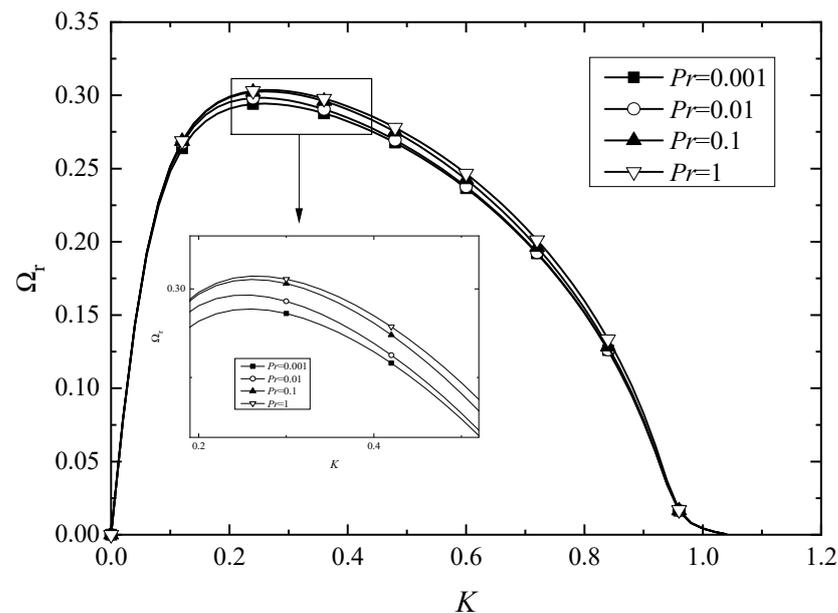

Figure 8. Effect of Prandtl number on the annular liquid jet instability when $Re = 5$ ($Re = 5$, $We_1 = 10$, $We_2 = 12.5$, $\gamma_1 = \gamma_2 = 0$, $\varepsilon_1 = \varepsilon_2 = 0.001$, $\Delta T^* = 0.2$, $\alpha = 1.25$, $Ma = 0.25$).

3.5. Effect of Heat Transfer Direction

The effect of the heat transfer direction on the annular liquid jet is also considered in the present study, and the dimensionless growth rate varying with the wave number is shown in Figure 10. It should be noted that the reason for the heat transfer is the temperature difference between the inner and outer gas phases. When the temperature of the outer gas is higher than that of the inner gas, heat transfer from the outer gas to the inner gas phase, We_2, is therefore larger than We_1, and $\Delta T^* > 0$. If the temperature of the inner gas is higher than that of the outer gas, heat transfers from the inner to the outer gas phase, $We_1 > We_2$ and $\Delta T^* < 0$ ($\Delta T^* = (\overline{T}_2 - \overline{T}_1)/\overline{T}_0$), respectively. The results in Figure 10 suggest that when the Weber number is small, the annular liquid jet tends to be more unstable when heat transfers from the outer to the inner gas phase. However,

heat transfer from the inner to the outer gas phase can enhance the annular liquid jet instability when the Weber number is very large. Therefore, to make the annular liquid jet breakup easily, it is necessary to consider the Weber number when heating the annular liquid jet—the temperature of the inner gas should be higher than that of the outer gas when the Weber number is small or the temperature of the outer gas should be higher than that of the inner gas when the Weber number is large.
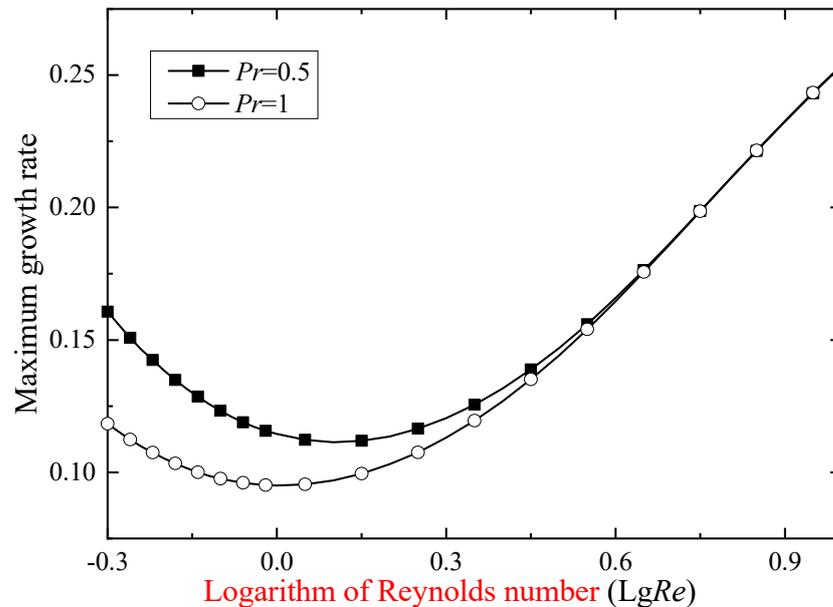

Figure 9. Variation in maximum growth rate with Re ($We_1 = 10$, $We_2 = 12.5$, $\gamma_1 = \gamma_2 = 0$, $\varepsilon_1 = \varepsilon_2 = 0.001$, $\Delta T^* = 0.2$, $\alpha = 1.25$, $Ma = 0.25$).
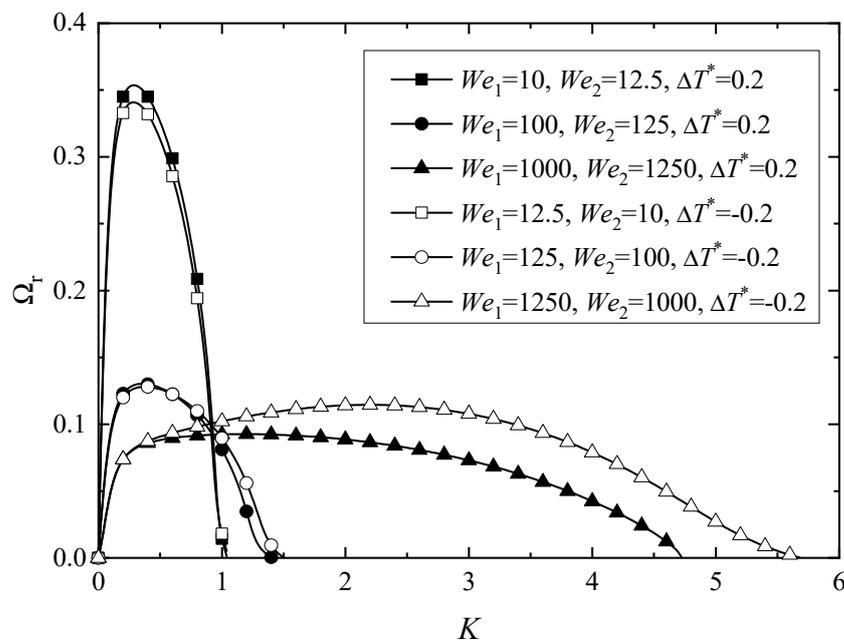

Figure 10. Effect of heat transfer direction on the annular liquid jet instability ($Re = 25$, $\gamma_1 = \gamma_2 = 0$, $\varepsilon_1 = \varepsilon_2 = 0.001$, $Pr = 0.5$, $\alpha = 1.25$, $Ma = 2.5$).

3.6. Effect of the Reynolds Number

The effect of the Reynolds number on the instability of an annular liquid jet is relatively complex. The Reynolds number is defined as the ratio of inertial force to viscosity

force. It can be clearly seen in Figure 9 that the maximum growth rate decreases with an increased Reynolds number when the Reynolds number is lower than the critical value, and then it increases. Zhang et al. [24] have reported this phenomenon on the thermocapillary instability of a liquid sheet. When the Weber number equals 1000, as shown in Figure 11, the thermocapillary effect also makes the annular liquid jet more unstable, and the maximum growth rate decreases when the Reynolds number varies from 0.5 to 1.25 when the wavenumber is small. In addition, the maximum growth increases with an increased Reynolds number when the Reynolds number is larger than 2.5. When the Reynolds number is small, which has been reported by Zhang et al. [24], the effect of surface tension becomes weaker than that of the viscosity; i.e., the enhancing effects of decreasing surface tension dominate the damping effects of viscosity; therefore, the instability of the annular liquid jet is enhanced.
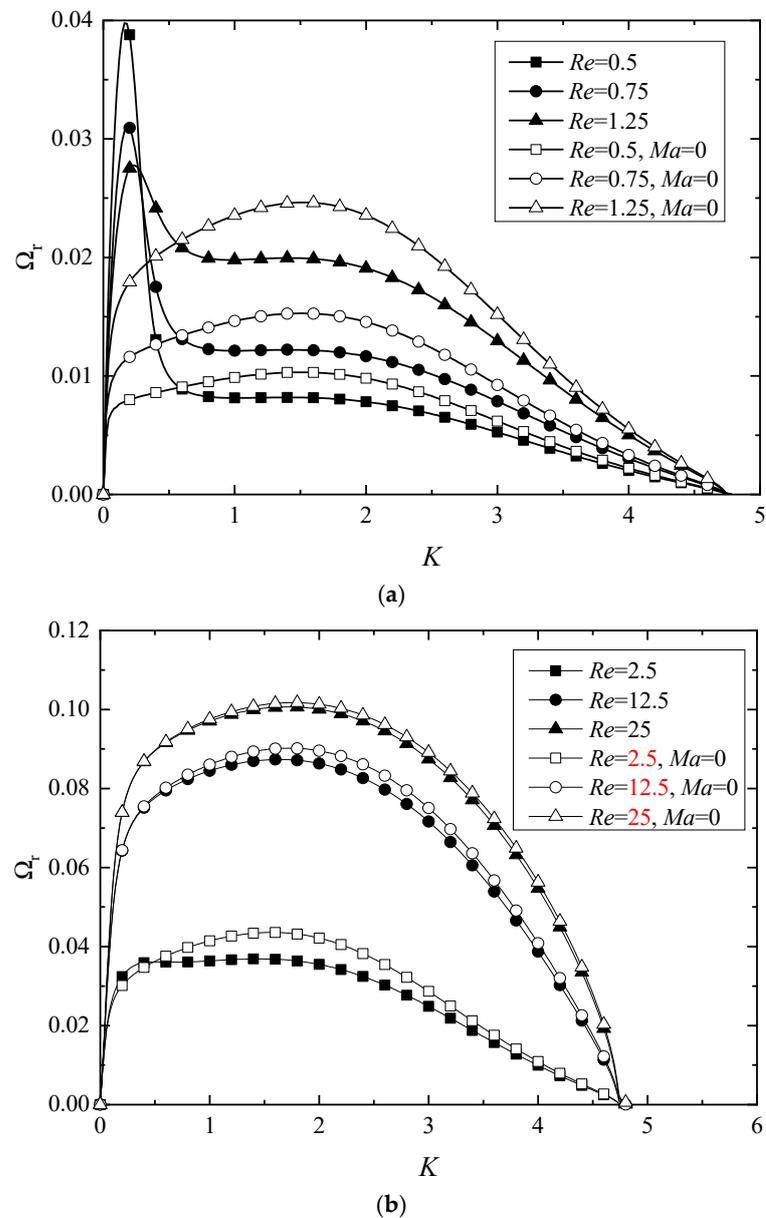

(**a**)

(**b**)

Figure 11. Effect of Reynolds number on the annular liquid jet instability when Weber number is large (We_1 = 1000, We_2 = 1250, $\gamma_1 = \gamma_2$ =0, $\varepsilon_1 = \varepsilon_2$ = 0.001, Pr = 0.5, α = 1.25, Ma = 0.25, ΔT^* = 0.2). (**a**) For a low Reynolds number. (**b**) For a large Reynolds number.

3.7. Effect of Temperature Gradient

In the present study, the dimensionless expression of the temperature gradient in an annular liquid jet is as follows:

$$\lambda^* = \frac{\Delta T^*}{r^* \ln \alpha} \tag{28}$$

It can be clearly seen in Equation (28) that the temperature difference ΔT^* is a factor that affects the temperature gradient in an annular liquid jet. Although temperature difference ΔT^* variation will change the Weber number, the temperature gradient also affects the instability of an annular liquid jet through the energy balance equation (Equation (10)). Hence, the Weber numbers of the inner and outer interfaces are assumed unchanged with temperature difference ΔT^* variation by modifying the program. The effects of the temperature difference are shown in Figure 12, with dimensionless temperature difference increasing from 0.1 to 0.5 and other parameters being constant; the maximum growth rate increases while the range of the unstable wave number hardly changes. It can be concluded that an increasing temperature difference, which increases the temperature gradient, enhances the instability of the annular liquid jet.
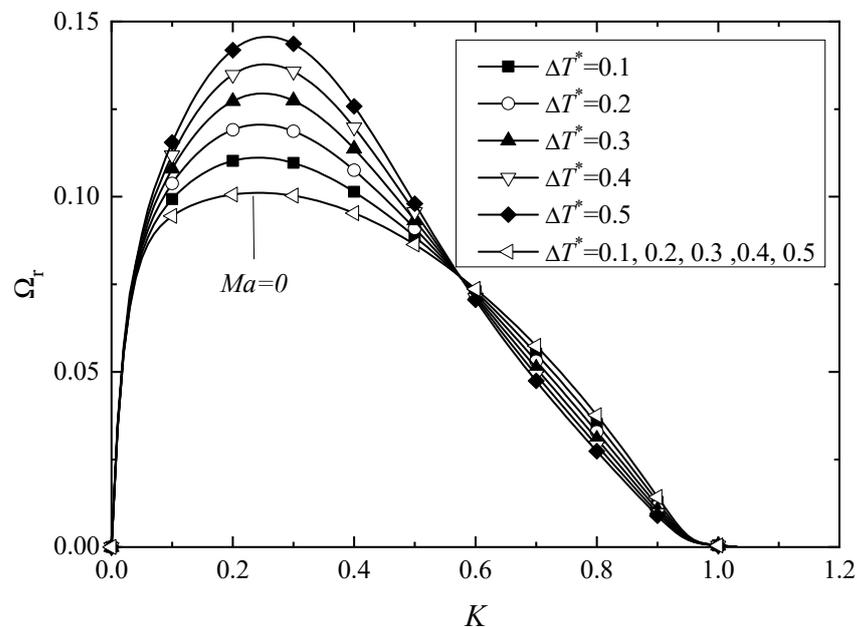

Figure 12. Effect of temperature difference ($We_1 = 10$, $We_2 = 12.5$, $Re = 0.5$, $\gamma_1 = \gamma_2 = 0$, $\varepsilon_1 = \varepsilon_2 = 0.001$, $Pr = 0.5$, $\alpha = 1.25$, $Ma = 2.5$).

3.8. Effect of Gas-to-Liquid Density Ratio and Velocity Ratio

The effects of the gas-to-liquid density ratio are also considered. The maximum growth rate increases with an increasing gas-to-liquid density ratio as shown in Figure 13. In addition, Figure 14 shows the effect of the gas-to-liquid velocity ratio on the instability of an annular liquid jet; when velocity density increases, the maximum growth rate also increases. As the aerodynamic force of the gas medium, which can enhance instability, is related to gas density and velocity, the aerodynamic force increases with the gas-to-liquid density ratio or the velocity ratio increases. Hence, the gas–liquid interface tends to be more unstable when the gas-to-liquid density ratio or velocity ratio increases. This suggests that increasing the gas-to-liquid density ratio or the velocity ratio helps to promote the atomization of an annular liquid jet.
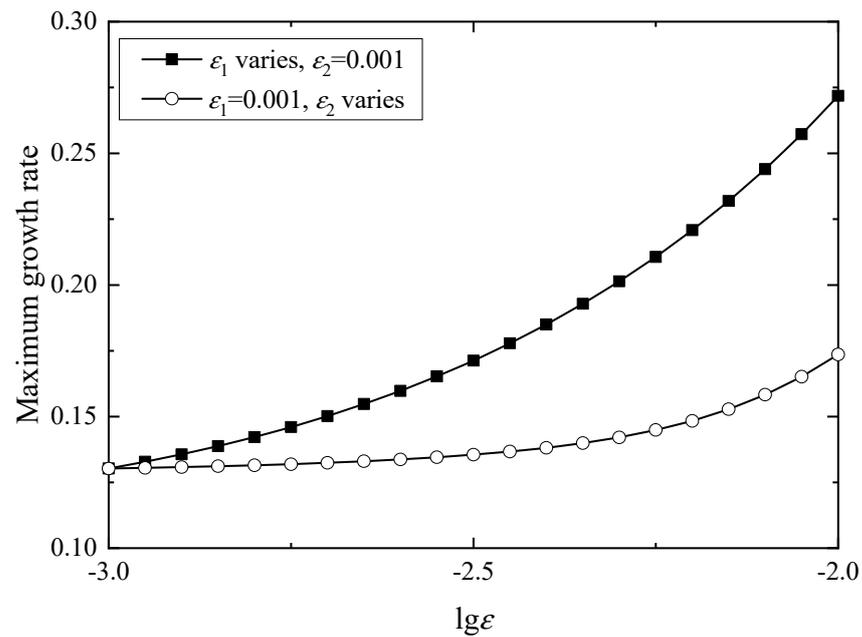
Figure 13. Effect of gas-to-liquid density ratio ($We_1 = 100$, $We_2 = 125$, $Re = 25$, $\gamma_1 = \gamma_2 = 0$, $Pr = 0.5$, $\alpha = 1.25$, $Ma = 2.5$, $\Delta T^* = 0.2$).
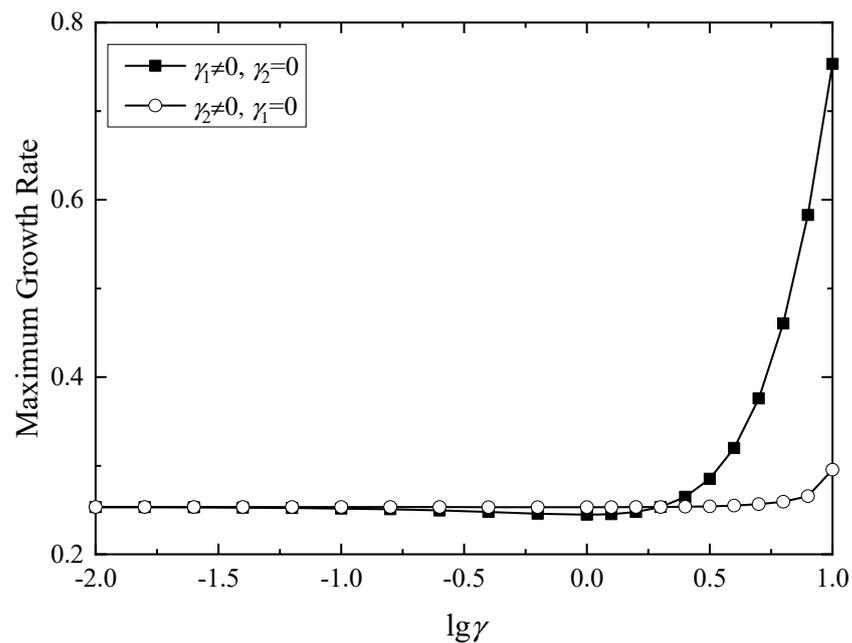

Figure 14. Effect of gas-to-liquid velocity ratio ($We_1 = 10$, $We_2 = 12.5$, $Re = 2.5$, $\varepsilon_1 = \varepsilon_2 = 0$, $Pr = 0.5$, $\alpha = 1.25$, $Ma = 0.25$, $\Delta T^* = 0.2$).

4. Conclusions

The temporal instability of an annular liquid jet surrounded by a gas medium with a radial temperature gradient was studied theoretically in this paper. The surface tension of the liquid phase is assumed as a function of the temperature. The spectral collocation method is used to obtain numerical solutions, and the accuracy of the program and the correctness of our results are verified to a certain extent by comparing them with the results of Shen and Li [4]; the results indicate two different unstable modes, namely, the "para-sinuous" mode and the "para-varicose" mode. As the annular liquid jet breaks up more easily in the "para-sinuous" mode than in the "para-varicose" mode, only the

"para-sinuous" mode is discussed. In this work, the effects of various dimensionless parameters on the instability of an annular liquid jet are indicated by the curves of growth rate variations with the wave number and physical parameters under different cases. There is a critical value of the Weber number: when the Weber number is lower than the critical value, decreasing the Weber number promotes instability, and increasing the Weber number enhances the annular liquid jet instability when the Weber number is larger than the critical value. According to the theoretical analysis, the Marangoni effect is related to the Weber number. The Marangoni effect enhances the instability of the annular liquid jet when the Weber number is small, and the annular liquid jet tends to be more stable when the Weber number is large. In addition, the effect of the Prandtl number depends on the Reynolds number and the Marangoni number, and increasing the Prandtl number has no effect on the instability of the liquid jet. Decreasing the Reynolds number makes the annular liquid jet more unstable when the Reynolds number is lower than a critical value, and increasing the Reynolds number increases the instability when the Reynolds number is larger than a critical value. The effect of the heat transfer direction is also discussed. Comparing the condition that heat is transferred from the inner to the outer gas phases, the annular liquid jet becomes more unstable when heat is transferred from the outer to the inner gas phases in the case of a small Weber number. In addition, heat transferred from the inner to the outer gas phases can enhance instability when the Weber number is large. Furthermore, the results show that a higher velocity difference across the inner interface is beneficial for sheet instability and that co-flowing gas streams will promote the atomization process when the gas velocities are relatively higher.

Institutional Review Board Statement: Not applicable.

Informed Consent Statement: Not applicable.

Data Availability Statement: Not applicable.

Conflicts of Interest: The authors declare no conflict of interest.

References

1. Sirignano, W.; Mehring, C. Review of Theory of Distortion and Disintegration of Liquid Streams. *Prog. Energ. Combust.* **1999**, *31*, 609–655.
2. Rayleigh, L. On the instability of jets. *Proc. Lond. Math. Soc.* **1878**, *10*, 4–13. [CrossRef]
3. Crapper, G.D.; Dombrowski, N.; Pyott, G.A.D. Kelvin–Helmholtz wave growth on cylindrical sheets. *J. Fluid Mech.* **1975**, *68*, 497–502. [CrossRef]
4. Shen, J.; Li, X. Instability of an annular viscous liquid jet. *Acta Mech.* **1996**, *114*, 167–183. [CrossRef]
5. Meyer, J.; Weihs, D. Capillary instability of an annular liquid jet. *J. Fluid Mech.* **1987**, *179*, 531–545. [CrossRef]
6. Chen, J.N.; Lin, S.P. Instability of an annular jet surrounded by a viscous gas in a pipe. *J. Fluid Mech.* **2002**, *450*, 235–258. [CrossRef]
7. Kang, Z.; Wang, Z.-G.; Li, Q.; Cheng, P. Review on pressure swirl injector in liquid rocket engine. *Acta Astronaut.* **2018**, *145*, 174–198. [CrossRef]
8. Anderson, W.E.; Yang, V. *Liquid Rocket Engine Combustion Instability*; American Institute of Aeronautics and Astronautics: Fort Collins, CO, USA, 1995.
9. Vadivukkarasan, M.; Panchagnula, M.V. Combined Rayleigh–Taylor and Kelvin–Helmholtz instabilities on an annular liquid sheet. *J. Fluid Mech.* **2017**, *812*, 152–177. [CrossRef]
10. Duke, D.; Honnery, D.; Soria, J. The growth of instabilities in annular liquid sheets. *Exp. Therm. Fluid Sci.* **2015**, *68*, 89–99. [CrossRef]

11. Yang, L.; Du, M.; Fu, Q. Stability of an annular power-law liquid sheet. *Proc. Inst. Mech. Eng. Part C J. Mech. Eng. Sci.* **2014**, *229*, 2750–2759. [CrossRef]

12. Fu, Q.-F.; Yang, L.-J.; Tong, M.-X.; Wang, C. Absolute and convective instability of a confined swirling annular liquid layer. *At. Sprays* **2014**, *24*, 555–573. [CrossRef]

13. Panchagnula, M.V.; Sojka, P.E.; Santangelo, P.J. On the three-dimensional instability of a swirling, annular, inviscid liquid sheet subject to unequal gas velocities. *Phys. Fluids* **1996**, *8*, 3300–3312. [CrossRef]

14. Reitz, R.D.; Lian, Z.W. The effect of vaporization and gas compressibility on liquid jet atomization. *At. Sprays* **1993**, *3*, 249–264. [CrossRef]

15. Cao, J.; Li, X. Stability of plane liquid sheets in compressible gas streams. *J. Propuls. Power* **2000**, *16*, 623–627. [CrossRef]

16. Yan, C.; Xie, M. Stability of an annular viscous liquid jet in compressible gases with different properties inside and outside of the jet. *Front. Energy Power Eng. China* **2009**, *4*, 198–204. [CrossRef]

17. Li, G.-B.; Wang, Y.-R.; Xiao, L.-M. Instability of an annular liquid sheet exposed to compressible gas flows. *Int. J. Multiph. Flow* **2019**, *119*, 72–83. [CrossRef]

18. Scriven, L.E.; Sternling, V.S. The Marangoni effects. *Nature* **1960**, *187*, 186–788. [CrossRef]

19. Funada, T. Marangoni instability of thin liquid sheet. *J. Phys. Soc. Jpn.* **1986**, *55*, 2191–2202. [CrossRef]

20. Oron, A.; Deissler, R.; Duh, J. Marangoni instability in a liquid sheet. *Adv. Space Res.* **1995**, *16*, 83–86. [CrossRef]

21. Dávalos-Orozco, L.A. Thermocapillar instability of liquid sheets in motion. *Colloids Surf. A* **1999**, *157*, 223–233. [CrossRef]

22. Tong, M.-X.; Yang, L.-J.; Fu, Q.-F. Thermocapillar instability of a two-dimensional viscoelastic planar liquid sheet in surrounding gas. *Phys. Fluids* **2014**, *26*, 33105. [CrossRef]

23. Fu, Q.-F.; Yang, L.-J.; Tong, M.-X.; Wang, C. Absolute and convective instability of a liquid sheet with transverse temperature gradient. *Int. J. Heat Fluid Flow* **2013**, *44*, 652–661. [CrossRef]

24. Zhang, S.; Lan, X.-D.; Zhou, M. Thermocapillary instability of a liquid sheet with centrifugal force. *J. Braz. Soc. Mech. Sci. Eng.* **2018**, *40*, 47. [CrossRef]

25. Ashgriz, N.; Mashayek, F. Temporal analysis of capillary jet breakup. *J. Fluid Mech.* **1995**, *291*, 163–190. [CrossRef]

26. Xu, J.-J.; Davis, S.H. Instability of capillary jets with thermocapillarity. *J. Fluid Mech.* **1985**, *161*, 1–25. [CrossRef]

27. Dijkstra, H.A.; Steen, P.H. Thermocapillary stabilization of the capillary breakup of an annular film of liquid. *J. Fluid Mech.* **1991**, *229*, 205–228. [CrossRef]

28. Li, S.; Yang, R.; Mu, K.; Luo, X.; Si, T. Thermal effects on the instability of coaxial liquid jets in the core of a gas stream. *Phys. Fluids* **2019**, *31*, 032106. [CrossRef]

29. Incropera, F.P.; Dewitt, D.P.; Bergman, T.L.; Lavine, A.S. *Fundamentals of Heat and Mass Transfer*; New Age International: New Delhi, India, 2006.

30. Joseph, D.; Funada, T.; Wang, J. *Potential Flows of Viscous and Viscoelastic Fluids*; Cambridge University Press: New York, NY, USA, 2008.

31. Funada, T.; Joseph, D.D. Viscous potential flow analysis of Kelvin-Helmholtz instability in a channel. *J. Fluid Mech.* **2001**, *445*, 263–283. [CrossRef]

32. Joshi, A.; Radhakrishna, M.C.; Rudraiah, N. Kelvin-Helmholtz instability in viscoelastic fluids in presence of electro-magnetic fields. *Phys. Fluids* **2011**, *23*, 094107. [CrossRef]

33. Tammisola, O.; Sasaki, A.; Lundell, F.; Matsubara, M.; Söderberg, L.D. Stabilizing effect of surrounding gas flow on a plane liquid sheet. *J. Fluid Mech.* **2011**, *672*, 5–32. [CrossRef]

34. Xie, L.; Yang, L.-J. Axisymmetric and nonaxisymmetric instability of a charged viscoelastic jet under an axial magnetic field. *J. Non-Newtonian Fluid Mech.* **2017**, *248*, 92–98. [CrossRef]

35. Duan, R.-Z.; Chen, Z.-Y.; Wang, C.; Yang, L.-J. Instability of a confined viscoelastic liquid sheet in a viscous gas medium. *J. Fluids Eng.* **2013**, *135*, 121204. [CrossRef]

36. Ye, H.-Y.; Yang, L.-J.; Fu, Q.-F. Spatial instability of viscous double-layer liquid sheets. *Phys. Fluids* **2016**, *28*, 102101. [CrossRef]

37. Xie, L.; Jia, B.-Q.; Cui, X.; Yang, L.-J.; Fu, Q.-F. Linear analysis and energy budget of viscous liquid jets in both axial and radial electric fields. *Appl. Math. Model.* **2020**, *83*, 400–418. [CrossRef]

38. Lin, S.P. *Breakup of Liquid Sheets and Jets*; Cambridge University Press: New York, NY, USA, 2003.